Holistically-Nested Edge Detection for AMD Images

Miriam Zipporah. B[1] & Dr. D. Francis Xavier Christopher[2]

[1]Research Scholar, Department of Computer Science,

Rathnavel Subramaniam College of Arts and Science, Coimbatore, Tamil Nadu, India

[2]Principal & Professor in Computer Science

SRM Trichy Arts and Science College, Tiruchirapalli, Tamil Nadu, India

DOI: www.doi.org/10.34293/iejcsa.v2i10.9

Abstract - *Macular degeneration associated with age is an eye disorder and is one of the leading causes of near blindness. Environmental and hereditary variables influence age-related macular degeneration (AMD) etiology. OCT (Optical Coherence Tomography) is the first quantitative ocular diagnostic for identifying eye illness. Accurate observation and comprehension of the condition are enhanced using CAD (Computer-Aided Detection) systems. This work aimed to develop a technique for Bruch's membrane, retinal pigment epithelium, and inner limiting membrane (ILM) segmentation in OCT images. The segmentation process combines the method using two deep neural networks, ResU-Net and HED. The conclusions reached were beneficial. The variation of U-Net is ResUNet the residual link is a kind of connection that enables the network to learn the residual rather than the complete mapping between the input and output. This method can improve network learning effectiveness and prevent the disappearing gradients issue. The deep learning model, called holistically nested edge detection (HED), performs image-to-image prediction using fully convolutional neural networks and intensely supervised nets. HED automatically creates extensive hierarchical representations to resolve ambiguity in edge and object boundary recognition (guided by intense supervision on side responses).*

INTRODUCTION

At least 2.2 billion human beings are thought to be visually impaired or blind, with at least 1 billion of those having some disability that might have been prevented or was not yet taken care of, judging by data from the World Health Organisation [1]. Age-related macular degeneration, glaucoma, cataracts, untreated refractive errors, and diabetic retinopathy are the five primary causes of blindness. A leading factor in vision loss in persons over 50 is age-related macular degeneration (AMD). The retina's macula, a tiny area that governs vision in the center, is harmed by AMD. The macula's loss of central, minute vision makes it challenging to engage in tasks like reading, driving, threading a needle, or identifying people [2]. Dry: Dry AMD is the most prevalent macular degeneration, accounting for around 80% of diagnosed instances. It is brought on by developing tiny yellow deposits under the macula. The progression of this type of AMD is typically very gradual, and symptoms may not appear until later. Wet: Developing new, small, frail blood vessels under and around the macula causes wet AMD.

These blood vessels are delicate, which makes it possible for them to burst and leak or bleed into the macula, damaging the retina and resulting in blindness. Wet AMD manifests more quickly and progresses to significant visual loss [2]. The retina is the innermost, light-sensitive eye layer that covers the back two-thirds. We divide it into ten layers; the neuroretina comprises the nine innermost layers, and the retinal pigment epithelium (RPE) is the outermost layer. The two separate kinds of light-sensitive photoreceptors, rods, and cones, which sense light in various environments, are found in the neuroretina. Between the RPE and the underlying choroid, Bruch's membrane (BM) serves as a sustaining barrier [3]. Druses are additional cells between Bruch's membrane layer and the retinal pigment epithelium layer (RPE). With advancing age, a certain amount of drusen is expected. However, the profusion of Drusen is a typical early sign of AMD [4].

The United States National Library of Medicine (NLM) claims AMD affects around 170 million individuals globally. As the percentage of senior persons rises, the prevalence rate is anticipated to grow during the following decades. The disease will impact two hundred eighty-eight million individuals by 2040 [5]. The retinal pigment epithelium (RPE) and drusen can be assessed using the optical coherence tomography picture. It has been demonstrated that the OCT is more sensitive to detecting pathological alterations related to AMD than the other advised tests. 57% of the analyzed eyes exhibited variations that could only be seen with OCT and not with other tests like angiofluoresceinography [6].

Age-related macular degeneration (AMD) is best detected early. Crucial for many reasons, including the possibility of preserving afflicted people's vision and quality of life. It can also substantially impact the condition's management and treatment. Some crucial elements of early diagnosis are Timely Intervention, Preservation of Functional Vision, Risk Factor Assessment, Patient Education and Counseling, Monitoring Disease Progression, Participation in Clinical Trials, and Vision Rehabilitation. With the visual analysis of the various images produced when this diagnosis is made using the OCT, and considering that a specialist attends and accompanies several patients each day, technological support for clinical practice is required to reduce evaluation errors.

As a result, we concentrate in this work on the segmentation of the ILM, RPE, and Bruch's membrane limits in OCT B-scan images of AMD and regular patients. The emphasis on these strata is due to two factors. The ILM layer is the retina's upper boundary, and the BM layer is its interior limit. Because of this, AMD can be diagnosed and seen in these layers, which can alter the retina's physiological properties and morphological structure. Being the outcome, we confirm the significance of segmenting these layers to aid in the identification and diagnosis of AMD. This paper suggests an automated technique for segmenting the retina's ILM, RPE, and BM layers in OCT B-scan pictures.

The four stages of the proposed approach are as follows: (a) pre-processing (enhancement, filtering); (b) defining the area of interest (using a variety of the processing of images techniques); (c) initial segmentation (relying on the ResU-net deep neural network (CNN) model); and (d) final segmentation (based on the HED deep neural network architecture for edge detection & classification). We recognize the following contributions of this work: Offering a solid technique that can automate the segmentation of the retina's layers. In total, there are five categories in this article. The results are displayed in Sections 4 and 5, Section 6 offers a synopsis of the process that was developed.

RELATED WORK

Age-related Macular Degeneration is a complicated image with a lot of noise and deformations brought on by pathologies, which alter the properties of the layer boundaries. Segmentation is needed for AMD (Age-related Macular Degeneration) images to isolate and identify the regions of interest within the macula accurately. AMD affects the macula, a small area in the retina's center that provides sharp and detailed central vision. Studies suggesting multiple methodologies for segmenting the borders of retinal layers have been noted.

A deep learning model based on UNet was indicated by the authors of a 2021 study [4] published in Computers in Biology and Medicine to segment AMD lesions in OCT images; the model achieved high accuracy.

Describe a method for automatically segmenting OCT pictures in [7]. Researchers provide a pipeline that includes a preprocessing phase that reduces speckle noise using the BM3D method.

[8] employed modified adaptive histogram equalization for image normalization and preprocessing to improve effective deep learning—developing and training a U-Net-based deep learning algorithm. An implication that defines the volume of the image is provided in [9]. As a result, areas that are pretty distant from the retina and make up of the image are not processed needlessly. The fundamental morphological image processing procedures, namely erosion, and dilation, are displayed in [10], demonstrating a promising avenue for digital image processing. The erosion procedure reduces the foreground depending on the structural elements. The dilation technique enlarges the foreground of the image. Thus, an image's noises can be removed using this approach.

In [11], the author outlines a clear concept and emphasizes the significance of segmenting blood vessels on retinal pictures since this technique efficiently reduces noise and improves the readability of blood vessels on images.

In [12], the focus is on the two-dimensional OTSU algorithm. After applying the best aspects of various algorithms to the OTSU, the author suggests a plan for improving the algorithm and verifies its efficacy.

The authors of [13] indicated a deep learning architecture based on ResUNet; a 2020 study the journal of Medical Systems published segment AMD lesions in OCT images. The suggested model demonstrated remarkable accuracy with an average Dice coefficient of 0.925 and an average sensitivity of 0.932.

Zhang et al. in 2020[14] suggested a new U-Net variant dubbed "Residual-Attention UNet (RA-U-Net)" that merged the residual connection and attention method. Several retinal image datasets showed state-of-the-art performance from this approach.

The original HED article first presented a deep learning-based edge detection model with cutting-edge performance on edge detection benchmarks [15]. To capture edges at various scales and levels of complexity, the model utilized an FCN architecture with numerous side output layers. Although this article focused on broad edge detection, it also set the stage for possible AMD image analysis applications.

This study investigated using HED for automated AMD detection in retinal fundus pictures [16]. Before utilizing HED for edge identification, the researchers preprocessed the pictures, such as optic disc removal and image enhancement. The detection of drusen, a characteristic of AMD, was done next using edge maps. The study showed that employing HED as a component of an automated AMD screening system has promise.

In [17] Holistically-Nested Edge Detection is a deep-learning-based approach to detecting the edges in the image that overcomes the limitation of the traditional edge detection methods by learning edge features directly from the image data. It offers quality results and high accuracy and is suitable for various applications in image processing and computer vision.

According to previous studies, Holistically-Nested Edge Detection (HED) has excellent potential for AMD image analysis, particularly for automated screening and lesion segmentation. HED is suited for identifying AMD-related characteristics, including drusen and lesions, since it can record multi-scale edge information. This research shows the growing interest in using deep learning methods, such as HED, to assist in the early identification, diagnosis, and monitoring of AMD, advancing computer-aided diagnosis and treatment of this ailment that can result in loss of eyesight. All the works listed above use various graph search strategies to produce the final segmentation of the edges of the retinal layer. As mentioned above, the method shown in this research performs the final segmentation phase using a deep neural network with an edge detection focus.

MATERIALS AND METHODS

Pre-processing, defining the area of interest, first segmentation, and final segmentation (classification) are the four steps of the suggested method for segmenting the OCT images of the retinal layers (ILM, RPE, and BM). The process diagram is displayed in Figure 1.

IMAGE DATASET

Data sets relating to medical imaging, such as AMD images, are hosted on the well-known data science and machine learning platform Kaggle.

As mentioned above, the proposed research uses a dataset from Kaggle.

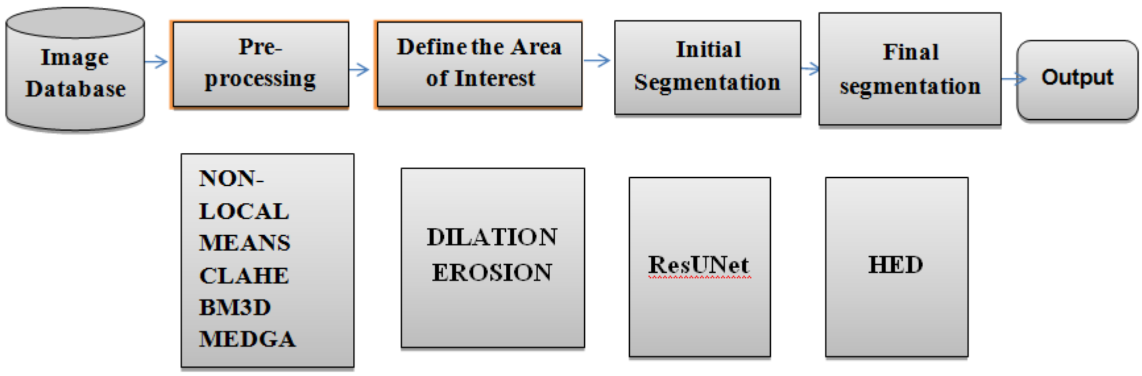

Figure 1: Flowchart of the Proposed Method

PRE-PROCESSING

The methods used to prepare data for analysis or machine learning models are called preprocessing [19]. It entails some procedures to convert raw data such that machine learning algorithms can read it quickly analyze or use. Data cleaning, Data normalization, Feature extraction, Data transformation, and Dimensionality reduction are a few standard preprocessing methods. We have suggested the following preprocessing techniques in this paper.

HISTOGRAM EQUALIZATION

A noteworthy contrast-enhancing method that works on practically all types of photos. In this work, the contrast limiting adaptive histogram equalization (CLAHE), which was developed in [19], is employed as an enhanced form of adaptive histogram equalization (AHE). CLAHE is a method for boosting contrast in visuals. The process involves breaking the image into smaller blocks, creating a histogram for each block, and then redistributing the pixel values per the histogram.

It stops noise from being amplified too loudly, as the AHE approach does. To lessen the noise issue, CLAHE employs a contrast amplification limiting technique for each neighboring pixel, generating a transformation function(1). In this instance, pixels will be dispersed uniformly as tiny (8*8) tiles. With the deployment of CLAHE, the thresholding value was determined. Figure 2 depicts the Histogram equalization based on CLAHE.

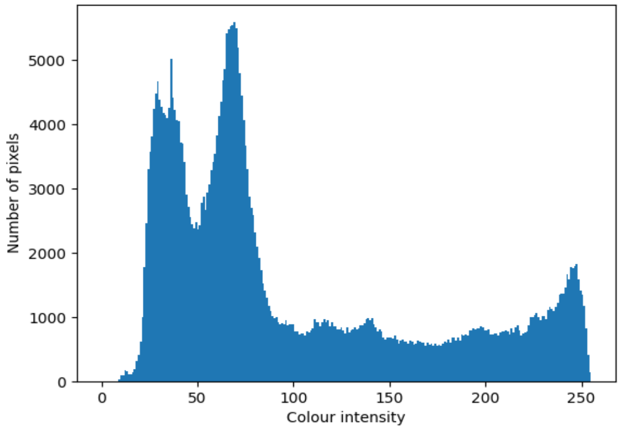

Figure 2: Histogram Equalization

The clip limit parameter, which determines the threshold for contrast limiting, must be considered while using CLAHE. 40 is the default value. The size of the tile grid determines how many tiles are in each row and column. The clip limit ranges from 0 to 1, with 0 denoting no contrast enhancement and 1 denoting the most significant contrast enhancement. CLAHE uses equation 1 to construct a histogram of the pixel values for each block of pixels in the image and then redistributes the pixels according to the histogram. The number of pixels allotted to each histogram bin depends on the clip limit. The surplus pixels are dispersed to other containers if the clip limit for a crate is reached.

THE NORMALIZED HISTOGRAM

Image Filtering

An essential procedure in image processing called filtering impacts spatial properties. The fundamental principle of filtering is to adjust each pixel's value dependent on its neighbors by applying a mathematical function, or kernel, to each pixel in the image. In image processing, various filter types are employed; we used BM3D filtering [20]. The foundation of the BM3D algorithm is a two-stage procedure. Similar picture blocks are found and grouped in the initial step.

Using a block-matching method, the most similar blocks are found by comparing each block to the others in the image. A set of reference blocks is then created by averaging similar blocks together. In the second stage, a collaborative filtering strategy is used to denoise each noisy block in the image. The similarity between the loud and reference blocks is the foundation for the denoising procedure. In a 3D transform domain, collaborative filtering is carried out. Correlations between the reference blocks are recorded using the block-wise 2D discrete cosine transform (DCT) and a third-dimensional transform. Images can be effectively denoised using BM3D, especially when the noise is random and uncorrelated [20]. Other picture restoration tasks, like super-resolution, deblurring, and compression artifact reduction, have also been added to their scope. Several criteria are frequently used to assess how well image-denoising algorithms function. The proposed method used the metric (2) listed below, and Figure 3 compares unprocessed and treated photos.

The following formula was used to determine PSNR:(2)

PSNR = 20 * log10(max_pixel_value / sqrt(MSE))

Here, the logarithm is base 10

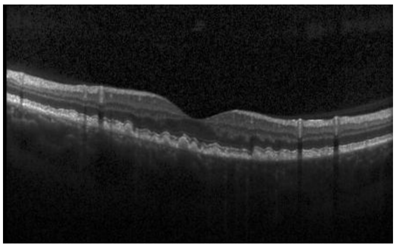

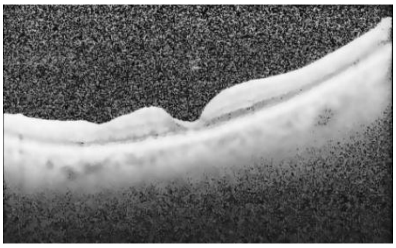

(a) (b)

Figure 3: (a) Non-Preprocessed and (b) Preprocessed

INITIAL SEGMENTATION

AMD photos can be processed using MedGA (Medical Genetic Algorithm) for various purposes, including feature selection, parameter tweaking, and model selection. In this study, we employed image classification [29]; MedGA was used to choose the most illuminating features from the AMD images and modify the hyperparameters of the classification model to improve performance. A set of components extracted from the AMD photos in this instance, coupled with labels indicating the amount of AMD severity, were the input to MedGA.

This characteristic is the criteria used to choose the best people from the population for the following generation. Two different selection procedures are frequently employed in MedGA. The proportionate fitness selection, also called the roulette wheel selection, was the type of selection used in our research. Genetic algorithms frequently employ this technique to choose members of the next generation based on fitness values. The following equation(3) states the likelihood of selecting person i from a group of N individuals:

P(i) = f(i) / sum(f(j)) for j = 1 to N (3)

where P(i) is the probability of choosing individual i, f(i) is the fitness value of individual i, and sum(f(j))is the total of each population member's fitness values. Finally, the region of interest in the image was extracted using this algorithm.

A popular image segmentation algorithm for thresholding grayscale images is Otsu's approach. It operates by determining the ideal threshold value that distinguishes between the foreground and background pixels in the embodiment according to their intensity levels. In some instances, Otsu's process may require producing more satisfactory results [12] due to irregular lighting, noise, or other visual artifacts. This issue was addressed with the 2D Otsu's technique, which extends Otsu's methodology to two-dimensional images.

A histogram of local gradient magnitudes rather than intensity values is used to determine the ideal threshold value in 2D Otsu's technique. This is because local gradient magnitudes provide more accurate information about the image's borders and contours, typically more critical for segmentation tasks than the image's overall intensity values.

A deep learning architecture called Residual U-Net (ResUNet) is used to segment medical images, particularly those for treating and diagnosing age-related macular degeneration (AMD) [14]. A Residual U-Net, also known as a Residual U-Net or R2U-Net is a variant of the U-Net architecture that includes residual connections. In contrast to learning the whole mapping, a residual relationship enables the network to remember the residual mapping between the input and output [28].

Dataset: From a public repository (Kaggle), the study used 100 optical coherence tomography (OCT) photographs of AMD patients. A spectral-domain OCT device (Heidelberg Spectralis, Heidelberg Engineering, Germany) with a resolution of 5.7 microns and a field of view of 20 x 20 degrees was used to obtain the images. Figure 3(a) displays the photos without any pre-processing operations applied.

Pre-Processing: Non-local means filtering (BM3D) and histogram equalization (CLAHE) was used to pre-process the OCT images to reduce noise and improve contrast. The pre-processed photos were resized to 512 by 512 pixels after that. The pre-processing processes used in this study are shown in Figure 1.

Model Architecture: The macula, optic disc, and blood vessels were among the various retinal layers and structures the ResUNet architecture segmented [28]. In the ResUNet architecture, the segmentation map was rebuilt by a decoder network after a series of residual blocks with skip connections. Age-related macular degeneration (AMD) pictures can be segmented using the Residual U-Net (ResUNet) architecture to identify the retina or drusen[14]. The ResUNet architecture, which contains residual connections between the encoder and decoder part of the model, expands the regular U-Net architecture (Figure 4 displays the basic architecture).

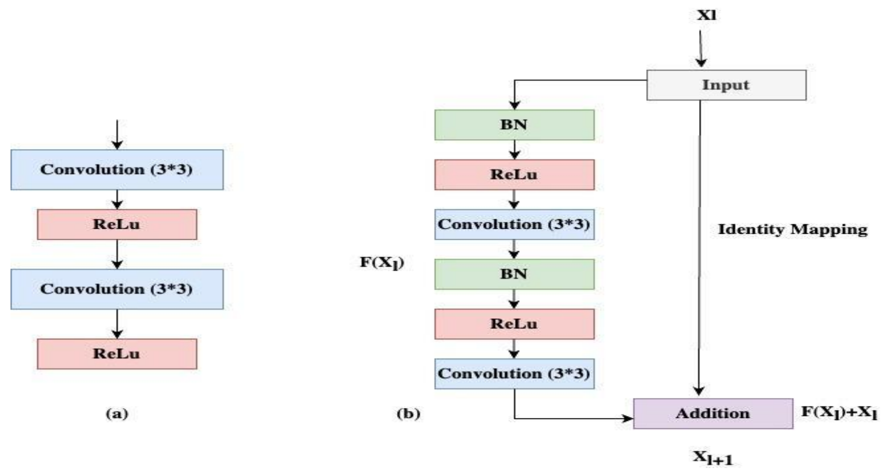

Figure 4: Building Blocks of Neural Networks (a) The Primary Neural Unit used in U-Net and (b) The Residual Unit with Identity Mapping are used in the Proposed ResUnet

Input Layer: The input image for this layer is a 2D or 3D image of the retina or the drusen. Residual Connections: These links between the model's encoder and decoder parts aid in maintaining spatial information and enhancing segmentation job performance.

Decoder: The ResUNet's decoder component consists of some upsampling layers that boost the spatial resolution of the features the encoder collected.

Output Layer: The output layer creates the segmentation map, a 2D or 3D image with the exact dimensions as the input image, and a class label for each pixel or voxel. A dataset of AMD images and the related ground truth segmentation maps can be learned by the ResUNet architecture. After training, the model produces a set of weights that may be applied to segment new images. It is crucial to remember that we can modify the design depending on the precise dataset and goal, and we can alter the number of layers and filters to accommodate the problem's complexity.

Considering the memory limits and computational cost when designing the architecture is crucial. The Deep Residual Network [28], or RESUNET, replaces the residual block with identity mapping for the convolution block used in UNET, which enhances the existing UNET architecture—resU-Net gains from residual learning and the UNET design.

There are no precise units of measurement for the metrics frequently used to assess medical image segmentation(Table 1), including the area under the receiver operating characteristic, sensitivity, specificity, and Dice similarity coefficient (DSC) (ROC) curve. Instead, they represent ratios, percentages, or dimensionless values that offer information about how well a model or algorithm works.

Table 1: Performance Evaluation of ResU-net Model

Metrics	Resunet Model	Range	Interpretation
Dice similarity coefficient (DSC)	0.93	0 (no overlap) to 1 (perfect overlap) for anticipated and ground truth masks	Identifies the degree to which the expected and actual segments match and are similar. A higher DSC suggests more accurate segmentation.
Sensitivity	0.95	1 (perfect sensitivity) to 0 (no true positives)	Indicates the percentage of real positive cases that the model adequately detected. Another name for it is true positive rate or recall.
Specificity	0.96	1 (perfect specificity) to 0 (no genuine negatives)	Denotes the percentage of real negative cases that the model successfully identified.
The receiver operating characteristic curve's ROC-AUC area	0.98	0 to 1	The ROC-AUC gauges how well a binary classification model performs overall at identifying positive and negative cases at various threshold levels. Better discrimination skills are indicated by a value that is nearer to 1.

FINAL SEGMENTATION

The HED (Holistically-Nested Edge Detection) method searches for edges in an input image using a deep learning-based model. It was first introduced in 2015 by Xie et al. The HED model is made to efficiently capture multi-scale edge information, producing outcomes in edge detection that are more precise and in-depth[15]. Edge detection is a crucial task in computer vision that includes locating and identifying abrupt discontinuities in an image. These visual discontinuities are frequently the starting point for more intricate computer vision techniques like object segmentation and object detection.[17].

Two critical problems are addressed by the proposed holistically nested edge detector (HED): For picture-to-image classification, holistic image training and prediction using fully convolutional neural networks (the system accepts an input image and immediately outputs an edge map image), Nested multi-scale feature learning is motivated by deeply-supervised nets, which apply deep layer supervision to preliminary classification results.HED is a potent edge detection method that uses the powers of FCNs and deep supervision to provide precise and thorough edge predictions in images[21].

In [24], lesion segmentation in AMD optical coherence tomography (OCT) images was investigated using HED. They devised a multi-task framework that used HED to segment various AMD-related diseases, including drusen, retinal fluid, and atrophy. The study demonstrated how well HED performed AMD lesion segmentation in OCT images. In this experiment[24], drusen and geographic atrophy, two AMD-related characteristics in fundus pictures, were automatically segmented using HED. The authors demonstrated the benefits of utilizing deep learning-based strategies for AMD feature segmentation by contrasting the performance of HED with that of other edge detection algorithms and conventional segmentation techniques. HED [24,25] could offer a useful deep-learning model for segmenting AMD layers in various medical pictures, including OCT images, according to the literature. HED-based models' excellent sensitivity and accuracy show their potential to help doctors identify and treat AMD. Below mentioned are the algorithm and architecture(Fig 5) that have been implemented in the proposed model. The HED algorithm uses multi-scale feature extraction and deep learning to perform cutting-edge edge detection.

It has successfully expanded the field of edge detection and has shown to be efficient in various computer vision applications. Key components and steps of the HED algorithm:

DATASET AND TRAINING

- The HED model is trained using a large dataset of images paired with corresponding ground truth edge maps. The model is covered under supervision. to learn the optimal edge-detection parameters and features.
- Network Architecture:

- HED employs a Fully Convolutional Network (FCN) architecture[15,26]. FCNs are designed to process images of arbitrary sizes and produce dense pixel-wise predictions.

Multi-Scale Feature Extraction

- The core idea of HED is to capture multi-scale information from the image to detect edges at different levels of complexity.
- The HED model uses multiple side output layers at different depths within the network to achieve this.

Side Outputs Fusion

- The side output layers with coarse edge maps are combined to create a comprehensive edge map.

Non-maximum Suppression

- After the fusion step, a non-maximum suppression technique is often applied to refine the final edge map.

Post-Processing (Optional)

- Depending on the application and use case, post-processing Techniques can be used to raise the standard of the edge map further.

Edge Map Visualization

- The final output of the HED algorithm is a pixel-wise edge map, where the value of each pixel shows whether something is there or not as an edge.

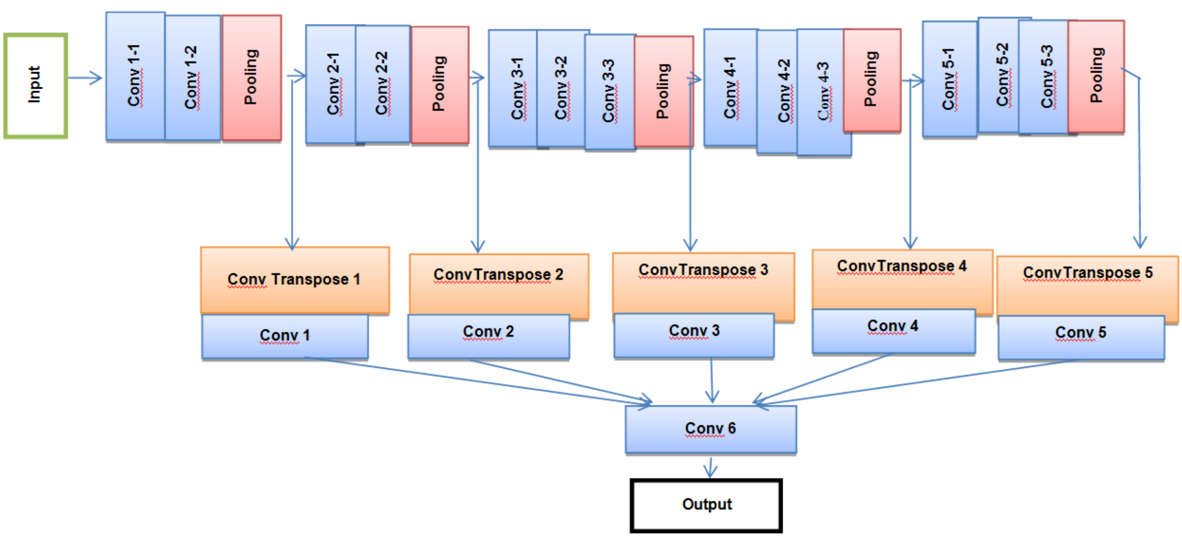

Figure 5: HED Network Architecture

Validation

Validating the findings is required after segmenting the margins of the retinal layers. In this study, the mean of the mean absolute error and the standard deviation (std) were employed as metrics frequently utilized in strategies to attain this goal. The precision of the retinal layer segmentation is measured by the MAE performance metric, which quantifies the absolute distances between the segmented layer's edge and the ground truth in each column of the picture. Equation 4 and 5 calculate the T OCT scan images' average value and standard deviation (size of m x n).

$$mean(X,Y)=1/T \sum_{t=1}^{1}(1/n \sum_{i=1}^{n} |X_t^i-Y_t^i|) \quad (4)$$

$$std(X,Y)=\sqrt{(1/T \sum)} \quad (5)$$

X_t^i is the point on the y-axis of the A-Scan in the t picture of OCT using the X technique, and X and Y are separate segmentation findings. X_t^i Y_t^i is the absolute positioning error on the y-axis in A-Scan i and B-Scan t. Y it is the position on the y-axis of A-Scan in the t OCT picture by the Y.

TRAINING AND TESTING

With the aid of the Keras deep learning package and TensorFlow-GPU as a backend, all tests were developed in Python. The OpenCV library was used to process images . A PC with an Intel I 7 processor, 128 GB of RAM, an 8 GB GeForce 1080 graphics card, and the Windows 10 operating system was used for training and testing. Training took about 360 s per epoch for the ResUnet model and 120 s for the HED Mode. The system runs for around two minutes with trained models, from the B-scan entry to the segmented layers' exit with quantification measures.

The selected hyperparameters for the following parameters were used throughout the training phase: 300 epochs, a batch size of 4, an Adadelta optimizer with an initial learning rate of 0.0001, and decay similar to 0.095, after multiple training sections and hyperparameter adjustment. We attempted to employ data augmentation in the trials to validate advancements made during the method's training stage. Layer segmentation could have been made better by expanding the sample set or by using transformations like Zoom, flip, and others. In some B-scan OCT pictures, a slight rotation could be visible.

The magnification actions (zoom, flip, rotation, and translation) cannot imitate the exam because there are few situations. Only intermediate AMD instances are present in the imaging database for the patients, limiting the method's applicability to subsequent phases of AMD.

RESULT & DISCUSSION

There were two groups created from the image dataset. OCT was divided into two groups: one for training with 308 volumes and the other for testing with 76 volumes. The distribution of exams with AMD and the control group in the base (269:115) was considered when choosing the data for each group. As a result, 88 volumes from the control group and 220 volumes with AMD made up the training set of images. The networks that make up the initial and final phases of segmentation were trained using it. Five B-scans from each volume of the training set, totaling 1540 images—540 of which were used for validation—were chosen to train the networks.

The most central B-scans were selected because they include complete marks of the edges of the retina layers. Each base volume has 100 B-scans, but not all have ground truth. 3,600 B-scans were assessed during the segmentation testing. The first segmentation step's goal is to distinguish between two regions of the image where the borders of the layers are present. The ILM's separation from the other two (RPE, BM) is demonstrated by the retina's structure, as discussed in Section 2 The ResU-net was employed for this work and produced the intended outcomes, scoring a 93% Dice on the test. Example of the outcome produced by the step is displayed in Fig 8. The results of determining the error between our method and the the outer edge of the BM, the inner edge of the RPE, and the ILM edge are shown in Table 2, along with the results. The graphic's color space and pixel density determine the Mean Squared Error (MSE) unit of measurement in the context of images. The square of the original units of the pixel values serves as the unit of measurement for the MSE metric, which is used to quantify the difference between two pictures “Intensity”in the context of digital images refers to a pixel's brightness or grayscale value. It describes a pixel's brightness or darkness. In an 8-bit per channel color space, the intensity values for grayscale images typically range from 0 (black) to 255 (white).Squaring the intensity value of a pixel is what is meant when we "I":(intensity)^2 = I * I

Table 2: The Results of Segmentation of the Boundaries of the Retinal Layers

Group	Edge	Mean Absolute Error	
		Mean	Std
AMD	ILM	0.49	0.10
	RPE	0.56	0.06
	BM	0.70	0.13
Control	ILM	0.48	0.08
	RPE	0.58	0.09
	BM	0.59	0.08
All	ILM	0.35	0.06
	RPE	0.40	0.05
	BM	0.52	0.07

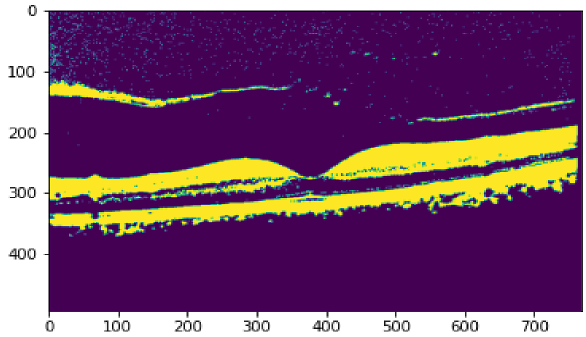

Figure 8: Example of Success Case

Both the dataset's ground truth and the automatic segmentation algorithm. Because drusen that produce deformations between these two layers are created in retinas with AMD, the average of the MAE is deemed low, with a larger value for the edges of the RPE and BM. Common standard deviation values in the findings indicated that the approach is very reliable across all classes.

Conclusion

When segmenting the borders of the retinal layers in OCT images, the suggested technique demonstrated excellent resilience. It is an entirely automated process. It is commonly acknowledged that this task is challenging. Using the same dataset, most investigations came up with less impressive results. The data set, which consists of OCT scans performed on individuals with intermediate AMD and healthy symptoms, is the one we employ in our study. The outcomes of this experiment are really encouraging. A comparison of the suggested strategy with other research that made use of the same image collection is shown in Table 3.

Table 3: Comparison with Related Works

Author	Method	Edge	Mean Absolute Error	
			Mean	Std
[30]	RNN-GS	ILM	0.38	0.92
		RPE	1.05	2.91
		BM	2.07	4.31
[30]	CNN-GS	ILM	1.10	7.21
		RPE	1.17	3.15
		BM	2.31	4.60
[30]	FCN-GS	ILM	0.65	4.24
		RPE	1.03	2.97
		BM	1.53	3.50
[31]	CapsNet	ILM	0.75	3.42
		RPE	0.93	0.86
		BM	1.09	2.49

[32]	DeepForest	ILM	0.47	0.12
		RPE	0.99	0.48
		BM	1.24	0.52
[33]	WAVE	ILM	0.68	4.09
		RPE	0.99	0.48
		BM	1.24	0.52
[4]	DexiNed	ILM	0.49	0.09
		RPE	0.57	0.07
		BM	0.66	0.12
Proposed	HED	ILM	0.35	0.06
		RPE	0.40	0.05
		BM	0.52	0.07

The suggested strategy has significant drawbacks despite outlining some advantages. The pre-processing stage, which uses enhancement and filtering, attempts to reduce the complexity of the dataset and the amount of noise in the images. However, the segmentation process still needs to be completed due to this. The method's performance is constrained by the picture base for AMD patients, which only includes intermediate instances. Deep learning models, like the CNNs utilized in this study, typically call for many parameters. For both models, we advise using hyperparameter defining and optimisation techniques to provide more honed architectures.

References

1. WHO. 2023, 'Blindness and vision impairment', World Health Organization.
2. IHBLIND. 'What is Age-Related Macular Degeneration (AMD)?', The Lighthouse for the Blind.
3. Liisborg, C. 2022, 'Age-related macular degeneration and myeloproliferative neoplasms – A common pathway', Acta Ophthalmologica, vol. 100, pp. 3-35.
4. Sous, JA, et al. 2021, 'Automatic segmentation of retinal layers in OCT images with intermediate age-related macular degeneration using U-Net and dexined', PloS One, vol. 16, no. 5, pp. 1-16.
5. Wong, WL, et al. 2014, 'Global prevalence of age-related macular degeneration and disease burden projection for 2020 and 2040: A systematic review and meta-analysis', The Lancet Global Health, vol. 2, no. 2, pp. e106-e116.
6. Eter, N & Spaide, RF. 2005, 'Comparison of fluorescein angiography and optical coherence tomography for patients with choroidal neovascularization after photodynamic therapy', Retina, vo. 25, no. 6, pp. 691-696.
7. Scharf, J, et al. 2021, 'Optical coherence tomography angiography of the choriocapillaris in age-related macular degeneration', Journal of Clinical Medicine, vol. 10.

8. Motozawa, N, et al. 2022, 'Automated evaluation of retinal pigment epithelium disease area in eyes with age-related macular degeneration', Scientific Reports, vol. 12.
9. Arslan, J, et al. 2021, 'Deep learning applied to automated segmentation of geographic atrophy in fundus autofluorescence images', Translational Vision Science & Technology, vol. 10, no. 8.
10. Shuo, H, et al. 2019, 'Image speckle noise denoising by a multi-layer fusion enhancement method based on block matching and 3D filtering', The Imaging Science Journal, vol. 67, no. 4, pp. 224-235.
11. Rubel, O & Lukin, V. 2018, 'Additive spatially correlated noise suppression by robust block matching and adaptive 3D filtering', Journal of Imaging Science and Technology R, c Society for Imaging Science and Technology, vol. 62, no. 6.
12. Ershov, EI, et al. 2021, 'A generalization of Otsu method for linear separation of two unbalanced classes in document image binarization', International Conference on Machine Vision Computer Optics.
13. Xu, X, et al. 2020, 'Automated age-related macular degeneration detection and lesion segmentation in optical coherence tomography images using deep learning', Journal of Medical Systems, vol. 44.
14. Zhang, J, et al. 2020, 'RA-U-Net: A Residual Attention U-Net deep convolutional network for retinal vessel segmentation', Journal of Healthcare Engineering.
15. Tutorials Point. 'Holistically-Nested Edge Detection with OpenCV and Deep Learning'.
16. Huang, H, et al. 2022, 'Glass defect detection via multi-scale feature fusion', Journal of Physics: Conference Series.
17. Chen, P, et al. 2016, 'Preprocessing and feature extraction for diagnosis of age-related macular degeneration', Journal of Medical Systems, vol. 40, no. 5.
18. Scharf, J, et al. 2021, 'Optical coherence tomography angiography of the choriocapillaris in age-related macular degeneration', Journal of Clinical Medicine, vol. 10.
19. Bhavyajain. 'Holistically-Nested Edge Detection with OpenCV and Deep Learning', Geeks for Geeks.
20. Shen, et al. 2018, 'Towards automated screening of age-related macular degeneration with HED'.
21. Lu, et al. 2019, 'Automatic detection of age-related macular degeneration in retinal fundus images using HED'.
22. Zhang, et al. 2020, 'HED-based lesion segmentation for age-related macular degeneration using optical coherence tomography'.
23. Maldonado, et al. 2021, 'HED for automatic segmentation of age-related macular degeneration features'.

24. Felt, V, et al. 2023, 'Fast ocean front detection using deep learning edge detection models', IEEE Transactions on Geoscience and Remote Sensing.
25. Xiang, D, et al. 2018, 'Automatic segmentation of retinal layers in OCT images with choroidal neovascularization', IEEE transactions on image processing.
26. Zipporah, BM, & Christopher, DFX. 2023, 'Residual U-Net architecture for retinal layers in oct images with choroidal neovascularization', SSRG International Journal of Electrical and Electronics Engineering, vol. 10, no. 5, pp. 205-212.
27. Rundo, L, et al. 2019, 'MedGA: A novel evolutionary method for image enhancement in medical imaging systems', Expert Systems with Applications, vol. 119, pp. 387-399.
28. Kugelman, J, et al. 2018, 'Automatic segmentation of OCT retinal boundaries using recurrent neural networks and graph search', Biomedical Optics Express, vol. 9, no. 11.
29. Santos, AM. 2019, 'Diagnosis of age-related macular degeneration from optical coherence tomography using geostatistics and capsule network'.
30. Chen, Z, et al. 2019, 'Automated retinal layer segmentation in OCT images of age-related macular degeneration', IET Image Processing, vol. 13, no. 9, pp. 1401-1411.
31. Lou, S, et al. 2020, 'Fast retinal segmentation based on the wave algorithm', IEEE Access, vol. 8.